Available online at www.sciencedirect.com
SCIENCE DIRECT®
Thermochimica Acta 402 (2003) 27–36
thermochimica acta
www.elsevier.com/locate/tca

Formation and characterization of samarium oxide generated from different precursors

G.A.M. Hussein [a,*], D.J. Buttrey [a], P. DeSanto Jr [a], A.A. Abd-Elgaber [b], Heba Roshdy [b], Ali Y.Z. Myhoub [b]

[a] *Department of Chemical Engineering, University of Delaware, Center for Catalytic Science and Technology, Newark, DE 19716, USA*
[b] *Chemistry Department, Faculty of Science, Minia University, El-Minia 61519, Egypt*

Received 5 June 2002; received in revised form 18 October 2002; accepted 20 October 2002

Abstract

$Sm(NO_3)_3{\cdot}6H_2O$ and $Sm_2(C_2O_4)_3{\cdot}10H_2O$ were used as precursors for the formation of Sm_2O_3. Thermal processes involved in the decomposition course of both salts up to 800 °C in air were monitored by nonisothermal gravimetry and differential thermal analysis. Intermediates and final solid products were characterized by IR-spectroscopy, X-ray diffraction and scanning electron microscopy. The results showed that $Sm(NO_3)_3{\cdot}6H_2O$ decomposes completely through nine endothermic mass loss processes. The dehydration occurs through the first four steps at 90, 125, 195, and 240 °C, culminating in a crystalline nitrate monohydrate, which subsequently decomposes to $Sm(OH)(NO_3)_2$ at 355 °C. The latter decomposes rapidly to form a stable and crystalline $SmO(NO_3)$ at 460 °C, through nonstoichoimetric unstable intermediates. Finally Sm_2O_3 forms at 520 °C. For the oxalate, the dehydration occurs in five steps: the anhydrous oxalate is thermally unstable and immediately decomposes to Sm_2O_3 at 645 °C through two unstable intermediates. The crystalline oxide obtained from the nitrate contains larger pores than the oxide obtained from the oxalate, as indicated from scanning electron microscopy (SEM) results.

Keywords: Sm oxide; Sm nitrate and oxalate; Formation; Characterization DTA, TG, IR, XRD and SEM

1. Introduction

Samarium sesquioxides, Sm_2O_3, with B-type centered monoclinic and C-type anion-deficient fluorite structures [1], have diverse applications in environmental and catalytic science [2–10]. It is important as a catalyst for dehydration of alcohols [3] and as a catalyst support for metals used in the dehydration of 2-alkanols to 1-alkenes, as well as for oxidative coupling of methane [3,5–7]. It is also used as a refractory oxide in the formation of ceramic cores for electrode applications [9–11]. Moreover, it is used for producing samarium–cobalt permanent magnets [12].

A review of thermal decomposition properties of rare-earth salts [13] reported that lanthanide oxides obtained from nitrate or acetate precursors exhibit higher surface areas than those obtained from oxalate precursors. Patil et al. [14] reported that the formation of M_2O_3 from rare-earth nitrates takes place via the oxy-nitrate ($MONO_3$). They also reported the possible formation of an anhydrous nitrate, whereas

* Corresponding author.
E-mail address: gma156@yahoo.com (G.A.M. Hussein).

0040-6031/03/$ – see front matter © 2002 Elsevier Science B.V. All rights reserved.
PII: S0040-6031(02)00535-X

Wendlandt and Bear [15] stated that the anhydrous nitrates are unstable. Studies on the decomposition of $Y(NO_3)_3{\cdot}5H_2O$ and $Y_2(C_2O_4)_3{\cdot}8H_2O$ indicated that a thermally stable monohydrate nitrate and dihydrate oxalate were formed [16]. Crystalline $YONO_3$ and $Y_2O_2CO_3$, respectively, were also detected by XRD. Y_2O_3 was the final product at 500 and 640 °C, respectively. The texture analysis by nitrogen adsorption and scanning electron microscopy (SEM) [17] revealed that Y_2O_3 obtained from $Y(NO_3)_3{\cdot}5H_2O$ at 500 °C has a higher surface area ($S_{BET} = 58\,m^2/g$) than that obtained at 700 °C from $Y_2(C_2O_4)_3{\cdot}8H_2O$ ($S_{BET} = 12\,m^2/g$), which was attributed to sintering.

The decompositon of $Pr(NO_3)_3{\cdot}6H_2O$ in air to form Pr_6O_{11} has been studied using TGA, differential thermal analysis (DTA), infrared spectroscopy (IR) and XRD [18]. The results indicated that $Pr(NO_3)_3{\cdot}6H_2O$ decomposes through 11 endothermic mass loss processes. Five dehydration steps occurred at 130, 180, 200, 230 and 250 °C, leading to the formation of crystalline nitrate monohydrate, which decomposes to $Pr(NO_3)_3$ at 340 °C. The latter, decomposes to Pr_6O_{11} at 465 °C via four different intermediates; $PrO(NO_3)$ at 430 °C, a nonstoichiometric unstable $Pr(O)_{0.25}(NO_3)_{2.5}$ at 362 °C; $Pr(O)_{0.5}(NO_3)_2$ at 382 °C; and $Pr(O)_{0.75}(NO_3)_{1.5}$ at 400 °C. The final decomposition product, Pr_6O_{11}, has a porous character with a large surface area of 46.3 m^2/g. Balboul [19] studied the decomposition course of $Ho(NO_3)_4{\cdot}5H_2O$ in air by TGA, DTA, IR, XRD, and SEM. It was reported that the anhydrous nitrates are thermally unstable and decomposition at 560 °C yielded Ho_2O_3. Different intermediates of nonstoichiometric oxy-nitrates were also detected.

The decomposition of $Sm_2(C_2O_4)_3{\cdot}7H_2O$ has been studied in air by Moosath et al. [20] and Wendlandt [21]. Both agree that partial decomposition occurs at 400 °C and that the final decomposition to Sm_2O_3 occurs at 700 °C. Above 400 °C the decomposition occurs gradually as the temperature increases to 700 °C. Although Moosath et al. [20] reported no lower hydrate or carbonate intermediates, Wendlandt reported the formation of a lower hydrate.

Recently, Hussein et al. [22] studied the decomposition of $Gd_2(C_2O_4)_3{\cdot}10H_2O$ to form Gd_2O_3 up to 800 °C in air. The results showed that $Gd_2(C_2O_4)_3{\cdot}10H_2O$ dehydrates in six endothermic steps, then decomposes to Gd_2O_3 at 575 °C through different intermediates. $Gd_2(C_2O_4)_3{\cdot}2H_2O$ and $Gd_2O_2CO_3$ were found to be stable intermediates, while the anhydrous oxalate was thermally unstable. The final product Gd_2O_3 had a surface area of 23.4 m^2/g.

The present investigation set out to characterize the thermal decomposition course of $Sm(NO_3)_3{\cdot}6H_2O$ and $Sm_2(C_2O_4)_3{\cdot}10H_2O$ to form Sm_2O_3 by means of thermogravimetric analysis (TG) and differential thermal analysis (DTA). The reaction products were characterized by infrared spectroscopy (IR) and X-ray powder diffraction (XRD). The progressive morphological development of Sm_2O_3 was followed using scanning electron microscopy (SEM).

2. Experimental

2.1. Materials

Samarium nitrate hexahydrate, $Sm(NO_3)_3{\cdot}6H_2O$, abbreviated as SmNit, was used as received and was 99.9% pure (WAKO, Pure Chemical Industry, Japan). Calcination products were obtained by heating at various temperatures (200–600 °C) for 1 h in air. The calcination temperatures were chosen on the basis of the thermal analysis results. Prior to analysis, the calcination products were kept dry over silica gel.

Samarium oxalate decahydrate, $Sm_2(C_2O_4)_3{\cdot}10H_2O$, abbreviated as SmOx, was prepared from samarium acetate by dropwise addition of a hot 4% ammonium oxalate solution to a stirred, hot solution of samarium acetate dissolved in glacial acetic acid. The resulting solution was then neutralized to pH 7 with NH_4OH. The precipitates formed were left to stand at room temperature for 1 h, filtered off, washed with a diluted ammonium oxalate solution, and finally dried at 80 °C to constant weight [22]. The calcination products were obtained by heating at various temperatures between 200 and 800 °C in air for 1 h. The calcination temperatures were chosen on the basis of the thermal analysis results.

For the sake of simplicity, all products are denoted in the text by SmNit for the nitrate and SmOx for the oxalate, followed by the calcination temperature. Thus, SmNit600 indicates decomposition products of SmNit at 600 °C for 1 h. In the case of original specimens, the suffix Org. will be used in place of temperature.

2.2. Thermal analysis

Thermal analysis was performed with a MAC-Science Model DTA-TG2000 (Tokyo, Japan). Thermogravimetric analysis (TG) and differential thermal analysis (DTA) curves were recorded over a wide range of temperatures, up to 800 °C at a heating rate of 10 °C/min in flowing air at 50 ml/min. The sample size used in the TGA measurement was approximately 15 mg. Highly sintered α-Al_2O_3 was used as a reference material for the DTA measurements.

2.3. Infrared spectroscopy

IR spectra were obtained at a resolution of 4 cm^{-1} over the range 4000–400 cm^{-1} using a model FT/IR 410 JASCO (Japan). IR spectra of SmNit, SmOx, and the solid calcination products were obtained from thin (>20 mg/m^2), lightly loaded (<1%) KBr-supported discs.

2.4. X-ray diffraction

XRD powder patterns were obtained with a Philips 3520 diffractometer using a fixed copper anode generating Cu Kα radiation (λ = 1.5418 Å) as the X-ray source and equipped with a Ni-filter and graphite monochromator on the detector arm. The operational settings for all the XRD scans were: voltage = 40 kV; current = 30 mA; scan range 4–60° 2θ using a step size of 0.02° at 2 s per step. For identification purposes the relative intensities (I/I_0) and the d-spacings (Å) were compared with standard diffraction patterns in the ASTM powder diffraction file [23].

2.5. Scanning electron microscopy

SEM was performed using a JEOL JXA-840 SEM operating at 20 keV. Samples of SmNit, SmOx, and their respective calcination products were mounted separately on aluminum stubs, evacuated to 10^{-3} Torr, and precoated for 5 min in a sputter-coater with thin, uniform, gold/palladium film to minimize charging in the electron beam. The applied voltage was 1.2–1.6 kV.

3. Results and discussion

3.1. Samarium nitrate hexahydrate, SmNit, $Sm(NO_3)_3{\cdot}6H_2O$

3.1.1. Processes I–V

The DTA curve (Fig. 1A) shows an endothermic, mass-invariant process located at 70 °C (process I). A direct measurement of the melting point of SmNit was found to occur between 70 and 73 °C. The TG and DTA curves (Fig. 1A) indicated that processes II and III are overlapping, endothermic mass loss processes with maxima at 90 °C and 125 °C, respectively. Process II yielded a mass loss (ML) = 4.1% (Table 1) corresponding to the release of one moles of water, while process III yielded a total ML = 12.1% corresponding to the release of two more moles of water. Processes IV occurred at 195 °C with a total ML = 16.1% and process V occurred at 240 °C with a total ML = 20.4%. The ML observed for processes IV and V each corresponded to the release of one more mole of water. Hence, the dehydration process most likely proceeds as follows:

$$Sm(NO_3)_3 \cdot 6H_2OII\ (90\,^{\circ}C) \rightarrow Sm(NO_3)_3 \cdot 5H_2O$$

$$III\ (125\,^{\circ}C) \rightarrow Sm(NO_3)_3 \cdot 3H_2O$$

$$IV\ (195\,^{\circ}C) \rightarrow Sm(NO_3)_3 \cdot 2H_2O$$

$$V\ (240\,^{\circ}C) \rightarrow Sm(NO_3)_3 \cdot H_2O$$

In support, the IR spectrum of SmNit200 (Fig. 2A) is very similar to that obtained for untreated SmNit. It displays absorption bands at 1640 cm^{-1} (δ_{OH} of

Table 1
Thermal processes in the calcination of $Sm(NO_3)_3{\cdot}6H_2O$

Step	T_{max} (°C)	Observed ML (%)	Theoretical ML (%)	Composition
I	70		–	$Sm(NO_3)_3{\cdot}6H_2O$ (liquid)
II	90	4.1	4.08	$Sm(NO_3)_3{\cdot}5H_2O$
III	125	12.1	12.15	$Sm(NO_3)_3{\cdot}3H_2O$
IV	195	16.1	16.2	$Sm(NO_3)_3{\cdot}2H_2O$
V	240	20.4	20.25	$Sm(NO_3)_3{\cdot}H_2O$
VI	355	24.2	24.3	$Sm(NO_3)_3$
VII	405	36.7	36.5	$SmO_{0.5}(NO_3)_2$
VIII	445	42.5	42.61	$SmO_{0.75}(NO_3)_{1.5}$
IX	460	48.6	48.6	$SmONO_3$
X	520	60.5	60.7	Sm_2O_3

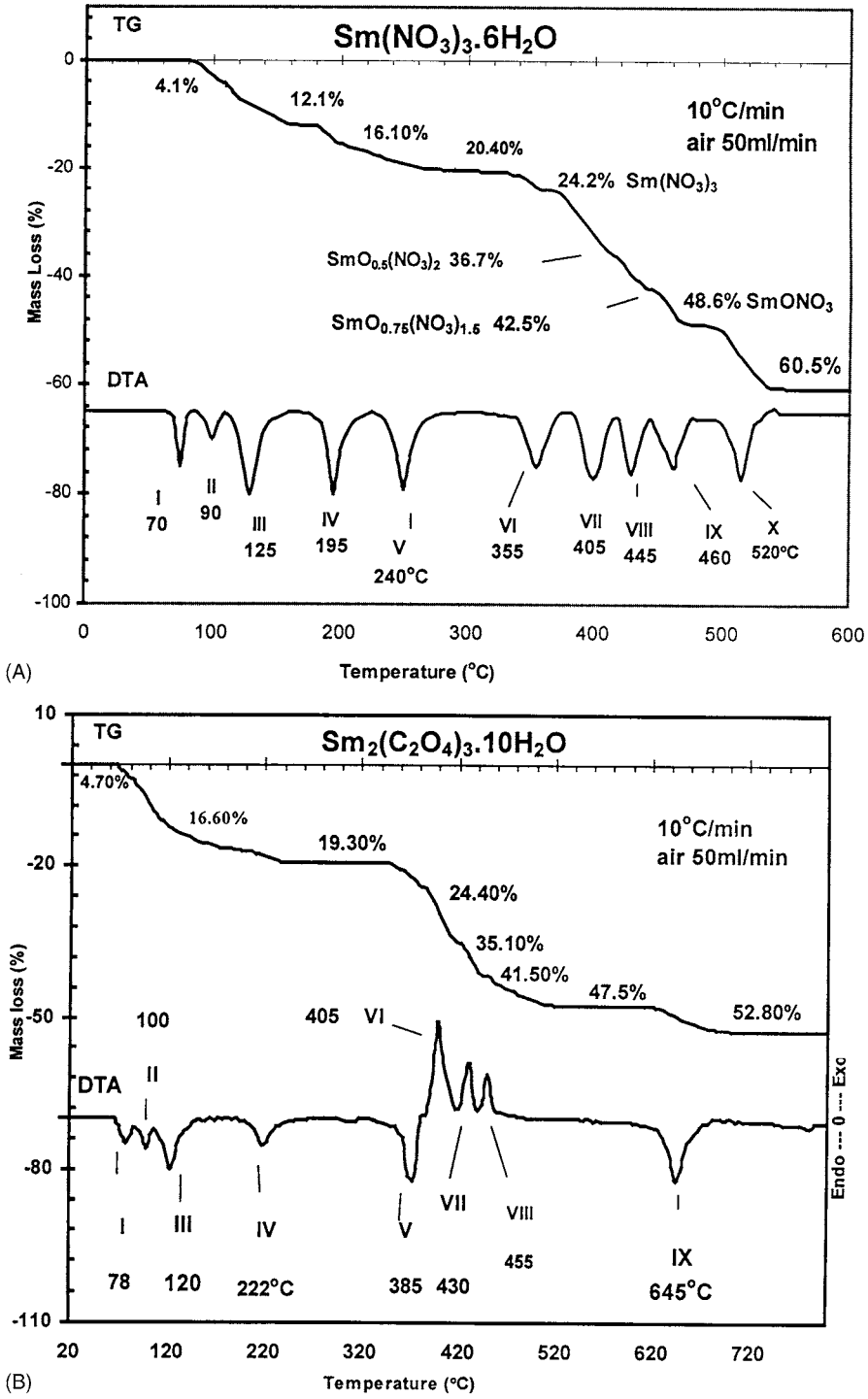

Fig. 1. TGA and DTA curves recorded for SmNit (A) and SmOx (B) at the heating rates indicated, in flowing air (50 ml/min).

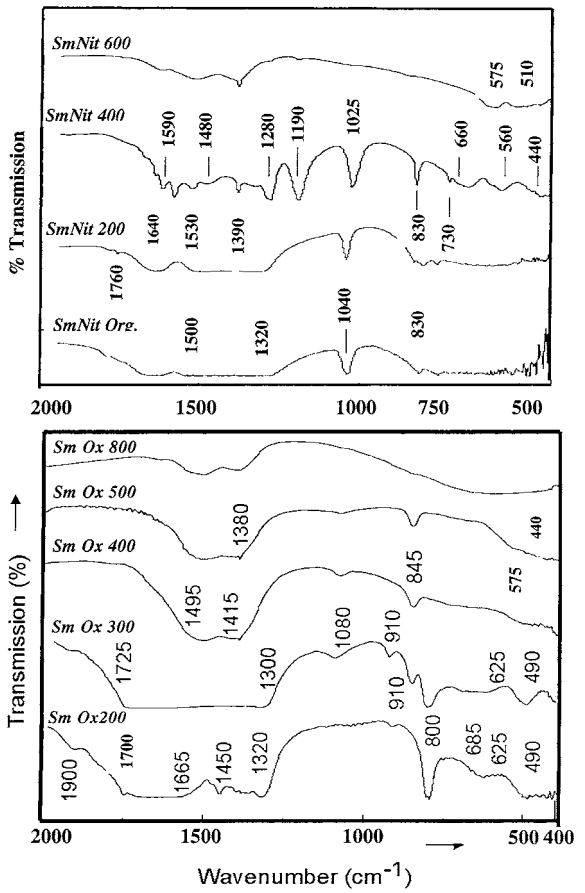

Fig. 2. IR-spectra for the 1-h calcination products of SmNit (A) and SmOx (B) at the temperatures indicated.

HOH) and at 1530–1320, 1040, 830 and 730 cm^{-1} due to the nitrate group in a mainly bidentate structure [24,25]. The XRD pattern of SmNit200 (Fig. 3A) indicates the formation of $Sm(NO_3)_3{\cdot}H_2O$ as a crystalline phase. Furthermore, the SEM of the parent SmNit (Fig. 4) reveals regularly-shaped crystals, while the SEM micrograph of SmNit200 (Fig. 4) shows large, irregularly-shaped crystals that exhibit evidence of a wet surface with holes and bulges as a result of melting and evolution of water vapour.

3.1.2. Processes VI–IX

Process VI is an endothermic ML process with a maximum at 355 °C and overlaps the succeeding processes (VII–IX). The mass loss determined for process VI is 24.28%, corresponding to the loss of the last mole of water and formation of anhydrous $Sm(NO_3)_3$. The strong overlap between processes VI and VII indicate that the anhydrous SmNit is thermally unstable. This is in agreement with previous studies, in which the anhydrous PrNit [18] and HoNit [19] are thermally unstable as well. The anhydrous SmNit is not detected, in agreement with Wendlandt and Bear [15], who also reported that the anhydrous nitrate is thermally unstable. Its clear that, the water of hydration is responsible for crystal coherency and thermal stability of SmNit.

Fig. 1A shows that processes VII–IX are overlapped, endothermic processes with maxima at 405, 445 and 460 °C (Table 1). The total ML associated with process VII is 36.7% close to the calculated 36.5% for the formation of $SmO_{0.5}(NO_3)_2$. For process VIII the total ML = 42.5%, close to the calculated 42.6% for the formation of $SmO_{0.75}(NO_3)_{1.5}$. Process IX leads to the formation of $SmONO_3$ as indicated from the observed weight loss of 48.6%, which matches the calculated value of 48.6% for this transition. Non-stoichiometric oxynitrates have previously been reported during the decomposition of PrNit [19], ThNit [26] and DyNit [27], while different $MO_x(NO_3)_y$ compounds were formed as unstable intermediates.

The IR spectrum of SmNit400 (Fig. 2A) provides convincing evidence for the formation of $SmONO_3$. Bridging nitro groups are indicated by new bands at 1190 and 850 cm^{-1} [24,25], possibly due to a combination of $\nu_{N=O}$ outside the bridge and bridging $\nu_{N=O}$, respectively. The strong composite absorption bands emerging at 600–400 cm^{-1} are probably related to metal–oxygen vibrational modes (Sm–O) [28]. Also the band due to δ_{OH} at 1640 cm^{-1} of $SmO(NO_3)$ is still present. Furthermore, the XRD pattern (Fig. 3A) of SmNit400 exhibits only diffraction peaks from $SmONO_3$.

The SEM image of SmNit400 (Fig. 4) shows irregularly stacked, sheet-like structures with steps, voids, and large cavities with rough surfaces, clearly different morphologically from the original SmNit and SmNit200.

3.1.3. Process X

Process X (Fig. 1A) represents endothermic decomposition of $SmONO_3$ at 520 °C. The total ML = 60.5% is close to the calculated 60.7% for the overall conversion of $Sm(NO_3)_3{\cdot}6H_2O$ to Sm_2O_3. The IR

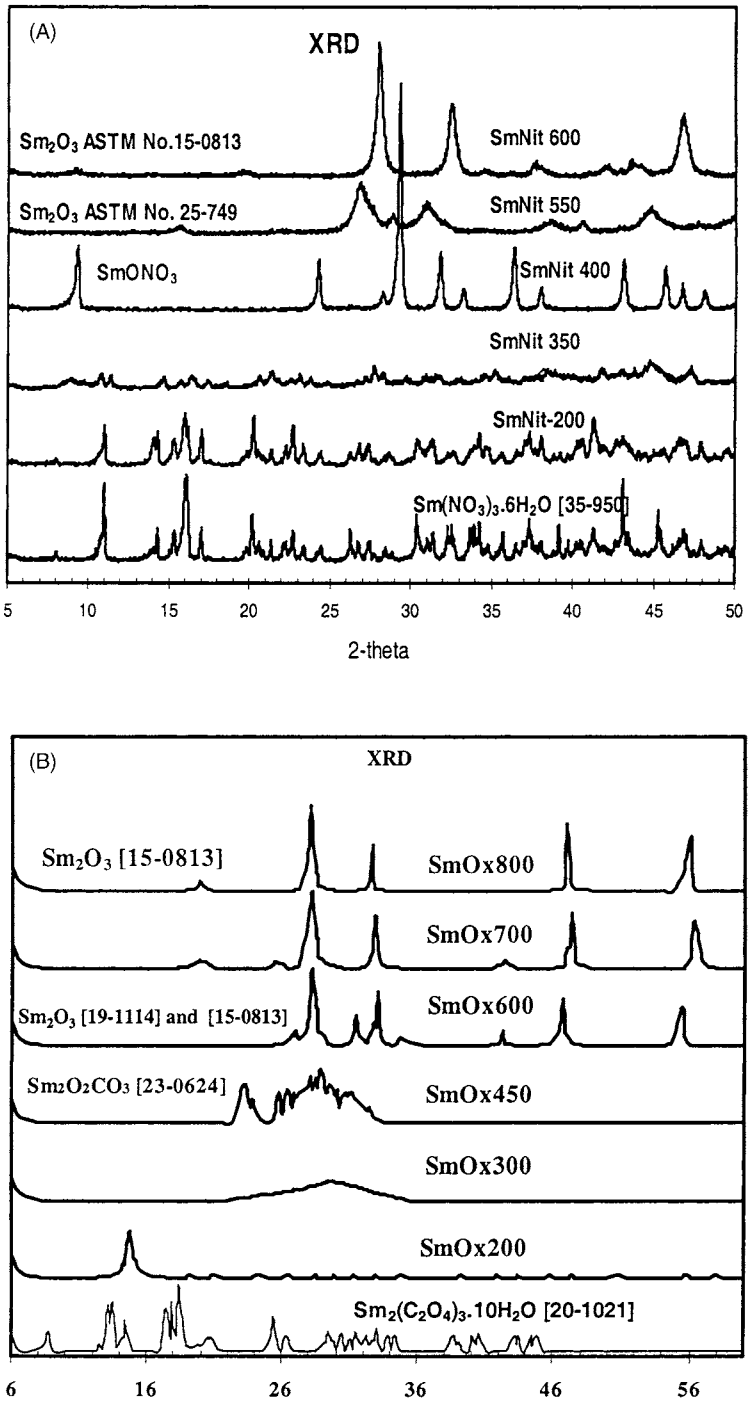

Fig. 3. X-ray powder diffractograms for the 1-h calcination products of SmNit (A) and SmOx (B) at the temperatures indicated.

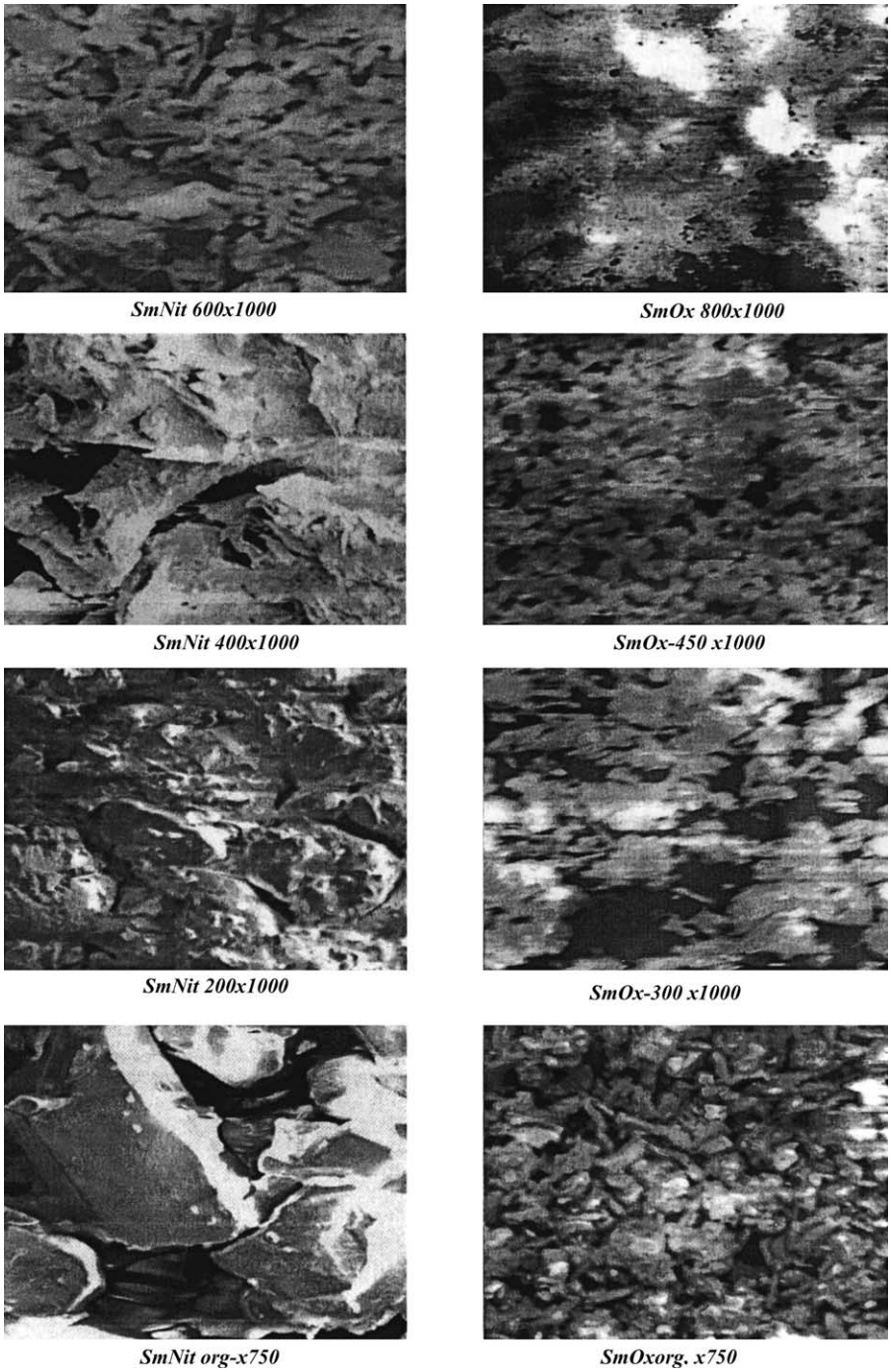

Fig. 4. Scanning electron micrograph obtained for SmNit and SmOx calcined at different temperatures for 1 h.

spectrum of SmNit600 (Fig. 2A) displays only bands below 800 cm^{-1} due to Sm_2O_3 [28]. Support for this interpretation is provided by the corresponding XRD pattern of SmNit550 (Fig. 3A) that compares well with the standard pattern (ASTM 25–749) of the monoclinic (B-type) Sm_2O_3 structure. However, the XRD pattern of SmNit600 (Fig. 3A) is of the cubic (C-type) structure (ASTM 15–0813), indicating that the monoclinic to cubic transformation occurs with heating in the range 550–600 °C. The SEM image of SmNit600 (Fig. 4) indicates that the morphology has changed; the sheet-like particles have grown together, although some pores, cracks, and fragments remain.

3.2. Samarium oxalate decahydrate, SmOx, $Sm_2(C_2O_4)_3{\cdot}10H_2O$

The TG and DTA curves in Fig. 1B reveal the presence of nine ML processes, designated I–IX, that occurred during the decomposition of $Sm_2(C_2O_4)_3{\cdot}10H_2O$ (SmOx) in an atmosphere of air. Three of these processes (VI, VII and VIII) are exothermic and overlap each other, while all the other processes are endothermic and resolved. The ML resulting from the first four processes (I–IV) suggests a step-wise dehydration of $Sm_2(C_2O_4)_3{\cdot}10H_2O$ leading to the formation of samarium oxalate dihydrate (Table 2). The first four processes result in the loss of eight moles of water with processes I and II removing two moles of water each, process III removing three moles of water, and process IV removing one mole of water.

In support of the above results, the IR spectra obtained for SmOx200 and SmOx300 (Fig. 2B) are both similar to that of untreated $Sm_2(C_2O_4)_3{\cdot}10H_2O$, displaying almost all of the characteristic absorption bands of oxalate anions between 1750 and 640 cm^{-1} [24,25], as well as those corresponding to the water of hydration. The XRD pattern of SmOx200 and SmOx300 (Fig. 3B) reveals the lack of crystallinity of the oxalate dihydrate intermediate. The SEM micrograph (Fig. 4) of samarium oxalate decahydrate reveals uniform small particles with nearly the same shape and morphology. The SEM micrograph of SmOx300 reveals some changes in the crystallite morphology as a result of decomposition to the oxalate dihydrate, specifically the particle size and degree of agglomeration have decreased relative to SmOxOrg. It seems likely that in the oxalate decahydrate, some of the water is present as water of crystallization that acts to stabilize the morphology, perhaps through an extensive hydrogen bonding network [26,27].

Table 2
Thermal processes in the calcination of $Sm_2(C_2O_4)_3{\cdot}10H_2O$

Step	T_{max} (°C)	Observed ML (%)	Theoretical ML (%)	Composition
I	78	4.7	4.8	$Sm_2(C_2O_4)_3{\cdot}8H_2O$
II	100	9.6	9.6	$Sm_2(C_2O_4)_3{\cdot}6H_2O$
III	120	16.6	16.9	$Sm_2(C_2O_4)_3{\cdot}3H_2O$
IV	222	19.3	19.3	$Sm_2(C_2O_4)_3{\cdot}2H_2O$
V	385	24.4	24.1	$Sm_2(C_2O_4)_3$
VI	405	35.1	35.4	$Sm_2(CO_3)_3$
VII	430	41.5	41.3	$Sm_2O(CO_3)_2$
VIII	455	47.5	47.2	$Sm_2O_2CO_3$
IX	645	52.8	53.1	Sm_2O_3

The dihydrate thus formed persists to 360 °C, at which temperature process V occurs endothermically with a maximum at 385 °C and total ML = 24.4% (Table 2), which is consistent with the expected 24.03% for the removal of 10 moles of H_2O from the oxalate decahydrate. This indicates that $Sm_2(C_2O_4)_3{\cdot}2H_2O$ is the only lower hydrate which is thermally stable. Fig. 1B also shows that after complete dehydration the decomposition takes place immediately through three overlapping exothermic processes. These processes show maxima at 405 °C for VI, 430 °C for VII and 455 °C for VIII (Table 2). Process VI brings the total ML to 35.1%, close to that calculated for the formation of samarium carbonate, $Sm_2(CO_3)_3$. Process VII is weakly exothermic and results in a total ML of 41.5%, corresponding to the formation of samarium monoxycarbonate, $Sm_2O(CO_3)_2$ (Table 2). Process VIII brings the total mass loss to 47.5%, which is close to the 47.2% total ML expected for the formation of $Sm_2O_2CO_3$ from the oxalate decahydrate.

The formation of $Sm_2O_2CO_3$ is supported by the IR spectrum (Fig. 2B) of SmOx400, which does not exhibit the δ_{HOH} absorption band of water that is present as a strong, broad absorption band in the IR spectra of SmOx200 and SmOx300. The fundamental modes of the CO_3^{2-} species between 1600 and 1300 cm^{-1} were present in SmOx400, as well as the absorption bands appearing at 800–400 cm^{-1}, which are related to the Sm–O vibrational lattice modes [28]. The characteristic bands of the oxy-carbonates are weaker as

the temperature goes up to 500 °C, as seen in the IR spectrum (Fig. 2B) of SmOx500, while all other Sm–O bands remain the same.

The XRD pattern (Fig. 3B) for the solid decomposition product of SmOx450 supports the TG (Fig. 1B) and IR (Fig. 2B) data. It reveals the formation of crystalline $Sm_2O_2CO_3$ (ASTM 23-0624). The corresponding SEM micrograph (Fig. 4) of SmOx450 reveals irregularly-shaped, large particles with rough surfaces that have a tendency to form relatively large agglomerates with large cavities and holes.

As the temperature is increased to 600 °C, process IX occurs endothermically with a total ML = 52.8%, which is close to the calculated 53.1% for the overall conversion of $Sm_2(C_2O_4)_3{\cdot}10H_2O$ to Sm_2O_3. This is confirmed by the IR-spectrum at 800 °C (Fig. 2B), in which absorption bands due to the oxy-carbonate species are no longer present. The absorption bands observed below 700 cm^{-1} are related to the lattice vibrational modes of Sm_2O_3. The weak bands around 1660, 1490 and 1410 cm^{-1} are most probably due to the surface contamination with carbonate and water.

The XRD pattern of the SmOx calcination product at 600 °C (FFig. 3B) provides further evidence for the complete formation of the oxide, as all diffraction peaks appearing in the XRD pattern correspond to the characteristic diffraction peaks of the two different crystalline Sm_2O_3 phases (monoclinic, ASTM no. 19-1114 and cubic, ASTM 15-0813). The XRD patterns of SmOx700 and SmOx800 indicate that only cubic Sm_2O_3 is present as expected (T_{max} = 645 °C). The SEM micrograph of SmOx800 also reveals that the Sm_2O_3 is well crystallized and shows large aggregates of particles with highly porous surfaces. It has previously been established that the release of volatile components creates a porous pathway through the material bulk [29,30].

4. Conclusions

The thermal decomposition of SmNit and SmOx in air to form Sm_2O_3 involves the following pathways.

$Sm(NO_3)_3{\cdot}6H_2O$:

$Sm(NO_3)_3 \cdot 6H_2O_{(s)}$ (70 °C)
→ $Sm(NO_3)_3 \cdot 6H_2O_{(l)}$ (90 °C)
→ $Sm(NO_3)_3 \cdot 5H_2O$ (125 °C)
→ $Sm\,(NO_3)_3 \cdot 3H_2O$ (195 °C)
→ $Sm\,(NO_3)_3 \cdot 2H_2O$ (240 °C)
→ $Sm(NO_3)_3 \cdot H_2O$(355 °C)
→ $Sm_2(NO_3)_3$ (405 °C)
→ $SmO_{0.5}(NO_3)_2$ (445 °C)
→ $SmO_{0.75}(NO_3)_{1.5}$ (460 °C)
→ $SmONO_3$ (520 °C) → Sm_2O_3

$Sm_2(C_2O_4)_3{\cdot}10H_2O$:

$Sm_2(C_2O_4)3 \cdot 10H_2O$ (78 °C)
→ $Sm_2(C_2O_4)_3 \cdot 8H_2O$ (100 °C)
→ $Sm_2(C_2O_4)_3 \cdot 6H_2O$ (120 °C)
→ $Sm_2(C_2O_4)_3 \cdot 3H_2O$ (222 °C)
→ $Sm_2(C_2O_4)_3 \cdot 2H_2O$ (385 °C)
→ $Sm_2(C_2O_4)_3$ (405 °C)
→ $Sm_2(CO_3)_3$ (430 °C)
→ $Sm_2O(CO_3)_2$ (455 °C)
→ $Sm_2O_2CO_3$ (645 °C) → Sm_2O_3

The oxalate dihydrate and nitrate monohydrate were found to be thermally stable. $Sm_2(NO_3)_3$ and $Sm_2(C_2O_4)_3$ were formed only as unstable intermediates in the decomposition of $Sm(NO_3)_3{\cdot}6H_2O$ and $Sm_2(C_2O_4)_3{\cdot}10H_2O$. The stable anhydrous intermediate in the decomposition of $Sm(NO_3)_3{\cdot}6H_2O$ was found to be $SmONO_3$, while $Sm_2O_2CO_3$ was found to be the stable anhydrous intermediate in the decomposition of $Sm_2(C_2O_4)_3{\cdot}10H_2O$. Finally, the Sm_2O_3 formed from $Sm(NO_3)_3{\cdot}6H_2O$ was observed to possess larger, more porous, sheet-like particles compared to Sm_2O_3 obtained from $Sm_2(C_2O_4)_3{\cdot}10H_2O$, which contained smaller particles in large aggregates with less porosity. Consequently, for catalytic purposes, samarium nitrate is a better precursor for the formation of Sm_2O_3 than samarium oxalate.

References

[1] P. Kofstad, Nonstoichiometry, Diffusion and Electrical Conductivity in Binary Metal Oxides, Wiley, New York, 1972, pp. 265–294.
[2] V.T. Amorebieta, A.J. Colussi, J. Am. Chem. Soc. 118 (42) (1996) 10236.

[3] M.J. Capitan, P. Malet, J.A. Odriozola, J. Phys. Chem. 97 (1993) 9233.
[4] K.D. Campbell, H. Zhang, J.H. Lunsford, J. Phys. Chem. 92 (1988) 750.
[5] Y.-L. Bi, K.J. Zhen, M.J. Jia, V. Corberan, Catal. Today 61 (2000) 369.
[6] H. Arakawa, Techno Jpn. 21 (1988) 23.
[7] K. Tanabe, K. Mismo, Y. Ono, H. Hattori, New Solid Acids and Bases, Elsevier, New York, 1989, pp. 41–47.
[8] G.A.M. Hussein, J. Chem. Soc., Faraday Trans. 90 (1994) 3693.
[9] S.C. Tsang, C. Bulpill, Sens. Actuators B Chem. 52 (1998) 226.
[10] F. Uchikawa, J.D. Mackenzi, J. Mater. Res. 4 (1989) 787.
[11] A.D. Berry, R.T. Holm, M. Fatemi, D.K. Gaskill, Mater. Res. 5 (1990) 1169.
[12] B. Gonzalvo, J. Romero, F. Frdenandez, M.J. Torralvo, J. Alloys Comp. 56 (2001) 323.
[13] G.A.M. Hussein, J. Anal. Appl. Pyrol. 37 (1996) 111.
[14] K.C. Patil, R.K. Gosavi, C.N.R. Rao, Inorg. Chem. Acta 1 (1967) 155.
[15] W.W. Wendlandt, J.L. Bear, J. Inorg. Nucl. Chem. 12 (1960) 276.
[16] G.A.M. Hussein, Thermchim Acta 244 (1994) 139.
[17] H.M. Ismail, G.A.M. Hussein, Powder Technol. 87 (1996) 87.
[18] G.A.M. Hussein, B.A.A. Balboul, M.A.A. Warith, A.G.M. Othman, Thermochim. Acta 369 (2001) 59.
[19] A. Basma, A. Balboul, Powder Technol. 107 (2000) 168.
[20] S.S. Moosath, J. Abraham, T.V. Swaminathan, Z. Anorg. Chem. 324 (1963) 90;
S.S. Moosath, J. Abraham, T.V. Swaminathan, Z. Anorg. Chem. 324 (1963) 103.
[21] W.W. Wendlandt, Analytic. Chem. 30 (1958) 56;
W.W. Wendlandt, Analytic. Chem. 31 (1959) 408.
[22] G.A.M. Hussein, M. Khedr, A.A. Farghali, Colloi Surf. 203 (2002) 137.
[23] J.V. Smith (Ed), X-ray Powder Data File, American Society for Testing Materials, Philadelphia, PA, 1960.
[24] K Nakamoto, Infrared Spectra of Inorganic and Coordination Compounds, Wiley, New York, 1970, p. 253.
[25] G.A. Gadsden, Infrared Spectra of Minerals and Related Inorganic Compounds, Butterworths, London, 1975, p. 65.
[26] G.A.M. Hussein, H.M. Ismail, Colloids Surf. 99 (1995) 129–139.
[27] G.A.M. Hussein, H. Korban, B. Goda, K. Miyaji, Colloids Surf. 125 (1997) 63–71.
[28] J.A. Goldsmith, S.D. Ross, Spectrochem. Acta A 23 (1967) 1909.
[29] G.A.M. Hussein, H.M. Ismail, Powder Tech. 84 (1995) 185.
[30] D.L. Trimm, A. Stanislaus, Appl. Catal. 21 (1986) 215.